MOLECULAR AND CELLULAR BIOLOGY, Dec. 2004, p. 10456–10469 Vol. 24, No. 23
0270-7306/04/$08.00+0 DOI: 10.1128/MCB.24.23.10456–10469.2004

Disruption of PLZP in Mice Leads to Increased T-Lymphocyte Proliferation, Cytokine Production, and Altered Hematopoietic Stem Cell Homeostasis

Francesco Piazza,† José A. Costoya, Taha Merghoub, Robin M. Hobbs, and Pier Paolo Pandolfi*

Cancer Biology and Genetics Program and Department of Pathology, Memorial Sloan-Kettering Cancer Center, Sloan-Kettering Division, Weill Graduate School of Medical Sciences, Cornell University, New York, New York

Received 8 July 2004/Returned for modification 19 August 2004/Accepted 1 September 2004

Deregulated function of members of the POK (POZ and Krüppel) family of transcriptional repressors, such as promyelocytic leukemia zinc finger (PLZF) and B-cell lymphoma 6 (BCL-6), plays a critical role in the pathogenesis of acute promyelocytic leukemia (APL) and non-Hodgkin's lymphoma, respectively. PLZP, also known as TZFP, FAZF, or ROG, is a novel POK protein that displays strong homology with PLZF and has been implicated in the pathogenesis of the cancer-predisposing syndrome, Fanconi's anemia, and of APL, in view of its ability to heterodimerize with the FANC-C and PLZF proteins, respectively. Here we report the generation and characterization of mice in which we have specifically inactivated the *PLZP* gene through in-frame insertion of a *lacZ* reporter and without perturbing the expression of the neighboring *MLL2* gene. We show that PLZP-deficient mice display defects in cell cycle control and cytokine production in the T-cell compartment. Importantly, PLZP inactivation perturbs the homeostasis of the hematopoietic stem and/or progenitor cell. On the basis of our data, a deregulation of PLZP function in Fanconi's anemia and APL may affect the biology of the hematopoietic stem cell, in turn contributing to the pathogenesis of these disorders.

The BTB/POZ (for bric à brac-tram track-broad complex/poxvirus zinc finger) domain is an evolutionarily conserved protein-protein interaction motif found at the NH_2 terminus of a group of transcriptional repressors containing DNA-binding Krüppel-like zinc fingers at their COOH termini (POZ and Krüppel or POK family proteins). This BTB/POZ domain mediates homo- and heterodimerization or oligomerization and is able to recruit corepressor multimolecular complexes, N-Cor/Sin3a/SMRT and histone deacetylases (HDACs), to target gene regulatory elements (1, 2). Deregulation of this mechanism has been implicated in the oncogenic activity of two BTB/POZ proteins involved in cancer, B-cell lymphoma 6 (BCL-6) in non-Hodgkin's lymphomas (17, 28) and promyelocytic leukemia zinc finger (PLZF) in acute promyelocytic leukemia (APL) (16, 18). PLZF fuses to retinoic acid receptor α (RARα) gene in the translocation t(11;17)(q23;q21), in rare cases of APL (10). As a result, two aberrant fusion proteins, PLZF-RARα and RARα-PLZF, are generated. In the PLZF-RARα molecule, the BTB/POZ domain of PLZF, by recruiting corepressor-HDAC complexes to RARα response elements, confers a constitutive repressive activity on RARα target genes, which become unresponsive to retinoic acid. Conversely, RARα-PLZF retains the ability to bind PLZF target sites on DNA through the PLZF domains and therefore potentially might deregulate PLZF-dependent gene expression (11, 26, 37).

Studies performed in our laboratory have shown that mice with a null mutation in the PLZF locus have limb and axial skeleton defects and display a homeotic transformation phenotype accompanied by altered expression of the HOX gene complex and of genes encoding bone morphogenetic proteins (3). We have demonstrated that PLZF regulates HOX genes through chromatin remodeling and bridging of distant regulatory sites within HOX regulatory elements (4). Inactivation of PLZF in PLZF-RARα transgenic models through the generation of compound $PLZF^{-/-}$/PLZF-RARα mutants unraveled the critical importance of PLZF functional disruption for the differentiation block at promyelocytic stage of myeloid differentiation normally observed in human APL (22). Strikingly, the consequences of PLZF inactivation are phenocopied by RARα-PLZF expression, as demonstrated in compound PLZF-RARα/RARα-PLZF transgenic mice, strongly supporting the dominant-negative function of RARα-PLZF over PLZF.

Searching for PLZF homologues, we identified a novel BTB/POZ protein that we named PLZP (for PLZF-like zinc finger protein) (35), which has also been described by other groups as FAZF (for Fanconi anemia zinc finger) (23), TZFP (for testis zinc finger protein) (27), and RoG (for repressor of GATA) (30). The PLZP protein has three C_2-H_2 Krüppel-type zinc finger domains, which display high homology with the three most C-terminal zinc finger domains of PLZF. PLZP has been shown to heterodimerize with FANC-C and PLZF proteins, and it has been therefore proposed to play a role in the pathogenesis of the autosomal-recessive bone marrow (BM) failure

* Corresponding author. Mailing address: Cancer Biology and Genetics Program and Department of Pathology, Sloan-Kettering Institute, Memorial Sloan-Kettering Cancer Center, Box 110, 1275 York Ave., New York, NY 10021. Phone: (212) 639-6168. Fax: (212) 717-3102. E-mail: p_pandolfi@ski.mskcc.org.

† Present address: Department of Clinical and Experimental Medicine, Clinical Immunology-Hematology Branch and Venetian Institute of Molecular Medicine, University of Padua, Padua, Italy.

or cancer-predisposing syndrome Fanconi's anemia and APL, respectively (23). However, the pathophysiological significance of these interactions is still obscure. The reported interaction between PLZP and PLZF suggests that they potentially regulate common target genes. Moreover, PLZP may bind similar DNA responsive elements as PLZF, due to the high degree of homology between the Zn finger domains. PLZP has also been shown to interact with other hematopoietic factors such as the GATA proteins. Mouse PLZP can repress GATA-3-dependent transactivation on cytokine promoters by displacing GATA-3 from its specific consensus sequences (30). Another report demonstrated interaction of human PLZP with GATA-2 through the zinc finger domain of PLZP, but the functional significance of this interaction is unknown (39). More recently, PLZP has been shown to be essential for the $CD8^+$-T-lymphocyte-specific repression of the IL-4 locus through recruitment of HDAC molecules (34). Mouse PLZP is also suggested to regulate transcription of the testis-specific Aurora kinase 1 gene (38). This could be of interest in view of recent reports that implicate PLZF in the maintenance of spermatogonial stem cells (14).

These various reports therefore suggest potential heterogeneous functions for PLZP. However, its in vivo physiological roles remain to be established. Furthermore, it still needs to be determined whether PLZF and PLZP exert distinct or redundant biological functions. To address these questions, we generated and characterized PLZP knockout mice which bear a null mutation in the PLZP locus.

MATERIALS AND METHODS

Targeting the mouse PLZP locus. We screened a 129/Sv strain mouse genomic library (Stratagene, La Jolla, Calif.) by using a [^{32}P]dCTP-labeled probe spanning the mouse PLZP exon 2 (generated by amplification of mouse testis cDNA with the primers EST2F (5′-GAGATGGCAGGAGCAACTAGG-3′) and EST2R (5′-ACTATGGGAGAAGGGAGCACC-3′) to isolate two genomic phagic clones containing the PLZP gene. These were subsequently subcloned in pBluescript KS plasmid (Stratagene) and characterized by restriction mapping and sequence analysis. To generate the PLZP-neo targeting vector, a 2.2-kb NdeI-NdeI fragment and a 3.1-kb KpnI-HindIII fragment from the genomic clones were subcloned in the pGK-Neo-pGK-TK (pPNT) vector as the 5′ and 3′ arms, respectively. To generate the PLZP-lacZ targeting vector, the NdeI-NdeI 2.2-kb fragment and a 2.9-kb NdeI-KpnI fragment were used as 5′ and 3′ arms, respectively, and subcloned in the pPNT vector, modified with the addition of the pACN cassette (8). The targeting vectors were linearized and electroporated into CJ7 129/Sv male embryonic stem (ES) cells, and colonies resistant to both G418 (350 μg/ml) and ganciclovir (2 μM) were expanded and screened by Southern transfer with a 3′ external probe by using EcoRI and XbaI digestions. Correctly recombined ES cell clones from PLZP-neo and from PLZP-lacZ transfections were further characterized by Southern transfer with a 5′ external and a NEO probe by using EcoRI digestion. Four independent ES clones from each transfection were used to generate chimeric mice, which transmitted the mutations to the germ line. F_1 heterozygotes (*PLZP*$^{wt/lacZ}$) were further analyzed by multiplex PCR on tail DNA to confirm the removal of the ACN cassette in the germ line. The PCR primers used for the analysis were CRE F (5′-TGATGGACATGTT CAGGGATC-3′), CRE R (5′-CAGCCACCAGCTTGCATGA-3′), 5P F (5′-T AACCTTACTGTGGGAAGACACC-3′), and 5P R (5′-CCAATCTGATCCTA AGCTGCTGCTCT-3′). A PCR strategy for genotyping PLZP *lacZ* utilized the primer pair PLZP F (5′-CTCCCTTCCCCTTCACAGGC-3′) and PLZP R (5′-ACAAAGGTCAGAATCTGAGC-3′), as well as lacZ R (5′-CGATTAAGTTG GGTAACGCC-3′).

Northern transfer and *lacZ* staining. For Northern blot analysis, total RNA was extracted from mouse testis tissues by using a TRIzol (Invitrogen/Life Technologies, Carlsbad, Calif.) solution according to the manufacturer's instructions. First, 10 to 20 μg of RNA was transferred onto a nitrocellulose filter and hybridized with a [^{32}P]dCTP-labeled probe corresponding to a BamHI-XhoI fragment of the mouse PLZP cDNA. For β-galactosidase (*lacZ*) staining, tissues were fixed in 4% paraformaldehyde for 2 h and then washed first in phosphate-buffered saline (PBS), followed by treatment with a washing buffer solution (2 mM MgCl, 5 mM EDTA, 0.01% sodium deoxycholate, 0.02% NP-40) and stained in X-Gal (5-bromo-4-chloro-3-indolyl-β-D-galactopyranoside) solution at 37°C overnight as described previously (29). The stained tissues were embedded in paraffin, sectioned, and counterstained with eosin. When single cell suspensions were used, fixation was performed in 2% formaldehyde–0.5% glutaraldehyde in PBS for 15 min at room temperature. The fixed cells were washed in PBS and stained in fresh X-Gal staining solution at 37°C overnight. The stained cells were washed, and cytospins were prepared and counterstained with eosin before analysis. To evaluate β-galactosidase activity by flow cytometry in stimulated lymphocytes (see below), cells were washed, resuspended at 10^6 cells/ml in prewarmed (37°C) staining buffer (PBS supplemented with 4% fetal calf serum and 10 mM HEPES [pH 7.2]), and incubated with 1 mM fluorescein di-β-D-galactopyranoside (FDG; Molecular Probes) at 37°C for 1 min. FDG loading in the cells was blocked by addition of ice-cold staining buffer containing 300 μM cloroquine. Cells were then analyzed on a FACScan.

Analysis of hematopoietic function. After administration of anesthesia, peripheral blood was withdrawn from the retro-orbital venous plexi of mice at 8 to 12 weeks, 6 months, and 12 months of age and collected into heparinized tubes. Complete hemograms were obtained by using an automated cell counter (Coulter Counter model ZF). Differential white blood cell counts were performed on slide smears. For morphological analysis of BM, cells were obtained from femur and tibia bones by flushing the marrow with Dulbecco modified Eagle medium by using a 27-gauge needle syringe, filtration through a cell strainer (40 μM), cytospin on glass slides, and staining with Wright-Giemsa. For hematopoietic colony assays, total BM cells (2×10^4) were plated in triplicate in 1 ml of 0.8% methylcellulose in Iscove modified Dulbecco medium containing fetal bovine serum, bovine serum albumin, human recombinant insulin, human transferrin, 2-mercaptoethanol, L-glutamine, recombinant murine interleukin-3 (IL-3), recombinant human IL-6, recombinant murine CF, and recombinant human erythropoietin (MethoCult; Stemcell, Seattle, Wash.). Colonies were scored for numbers of erythroid burst-forming unit, granulocyte-macrophage CFU, and granulocyte-erythrocyte-macrophage-megakaryocyte CFU (CFU-GEMM) after 6 and 12 days. For assessment of mitotic activity in the hemopoietic stem cell compartment, we used a four parameter fluorescence-activated cell sorting (FACS) analysis modified from a previous study (13). Briefly, BM cells were incubated in Hoechst staining buffer with Hoechst 34322 at 37°C for 30 min and then with Pyronin Y for a further 30 min. The cells were subsequently incubated with a cocktail of biotin-labeled antibodies against lineage markers (CD3, CD4, CD8, B220, Ter119, Gr1, CD11b, and NK.1), followed by APC-conjugated streptavidin- and fluorescein isothiocyanate-conjugated anti-Sca1 antibody. After a wash in PBS, the samples were analyzed by using a MoFlo flow cytometer at the Memorial Sloan-Kettering Cancer Center flow cytometry facility.

Analysis of T-lymphocyte function. Single cell suspensions from spleen and lymph nodes were depleted of red blood cells in lysis buffer (0.15 M ammonium chloride [NH_4Cl], 10 mM potassium bicarbonate [$KHCO_3$], 0.1 mM EDTA). Total $CD3^+$, $CD4^+$, and $CD8^+$ subpopulations were purified by negative selection by using MACS isolation kits according to the manufacturer's protocol (Miltenyi Biotech, Inc., Auburn, Calif.). For in vitro differentiation assays, purified $CD4^+$ lymphocytes (1.5×10^6/ml) were stimulated with 2 μg of plate-bound anti-CD3ε antibody and 2 μg of plate-bound anti-CD28 antibody/ml in the presence of IL-12 and anti-IL-4 or of IL-4, anti-IL-12, and anti-IFN-γ for Th-1 and Th-2 skewing conditions, respectively. Then, 100 U of IL-2/ml was added to the cultures after 48 h. After 7 days, cells were harvested, washed extensively, and restimulated with 75 ng of phorbol myristate acetate (PMA; Sigma-Aldrich)/ml and 1 μM calcimycin (Sigma-Aldrich) for 6 h, the last 3 h in the presence of monensin (BD Pharmingen). Cells were then fixed in 4% paraformaldehyde, permeabilized in PBS supplemented with saponin and 1% fetal bovine serum, and incubated with phycoerythrin (PE)-conjugated anti-cytokine or isotype control antibodies. For the proliferation assays, purified T lymphocytes from lymph nodes and spleens were stimulated in 96-flat well plates (10^5/well) with different concentrations of plate-bound anti-CD3ε antibody in the presence or absence of anti-CD28 antibody (1 μg/ml) and/or different concentrations of IL-2. At different time points, [^{3}H]thymidine (10 μCi/well) was added to the cultures for the last 12 h. The ^{3}H incorporation was evaluated by scintillation counting by using a top count β-counter (Microbeta Plus; Wallac).

CFSE labeling. CFSE (5,6-carboxyfluorescein diacetate, succinimidyl ester) was purchased from Molecular Probes (Eugene, Oreg.). The cells were washed with ice-cold PBS and resuspended at 5×10^6 cells/ml in ice-cold PBS. CFSE was kept as a 0.5 mM stock in dimethyl sulfoxide and stored at −20°C in a desiccator box. Cells were labeled by diluting the 0.5 mM CFSE stock 1,000-fold into the

cell suspension (final concentration, 0.5 μM) and incubating them for 10 min at 37°C. After labeling, fetal calf serum was added to 5% final concentration, and the cells were immediately centrifuged and washed with ice-cold PBS.

FACS analysis. Directly conjugated anti-CD4, CD8, CD3, B220, Gr1, Mac1, Ter119, CD71, and gamma interferon (IFN-γ) monoclonal antibodies (MAbs) were purchased from Pharmingen (San Diego, Calif.). To block nonspecific binding, single cell suspensions were preincubated with CD16/CD32 (Pharmingen) and then stained with specific antibody for 30 min at 4°C. Stained cells were washed and analyzed on a FACScan flow cytometer (Becton Dickinson). For the FACS sorting of BM cells, total BM cells were prepared as described above and stained with a cocktail of biotin-conjugated anti-lineage marker antibodies (Pharmingen). Fluorescein isothiocyanate-conjugated anti-Sca1 antibody was added in the second incubation step together with PE-conjugated streptavidin. Stained cells were washed in PBS and sorted by using either a MoFlo or FACS Vantage flow cytometer at the Memorial Sloan-Kettering Cancer Center flow cytometry facility. Sorted Lin^- $Sca1^+$ and Lin^+ $Sca1^+$ cells were subjected to *lacZ* staining and cytospun onto glass slides.

RNase protection assay. Total RNA was extracted from purified $CD4^+$ lymphocytes grown under the conditions described above or from $CD8^+$ lymphocytes stimulated for 48 h through T-cell-receptor (TCR) engagement with plate-bound anti-CD3ε antibody. RNase protection assay analysis was performed on 5 to 10 μg of total RNA by using the Riboquant kit (BD Pharmingen) according to the manufacturer's instructions. The mCK-1 template set was used in all of the experiments. Bands in RNase protection assays that corresponded to cytokine transcripts were quantified through use of a PhosphorImager and the ImageQuant program (Molecular Dynamics). Cytokine mRNA bands were normalized to the corresponding L32 mRNA standard bands in each lane.

Histology and immunohistochemistry. Testes from adult mice were fixed in formalin and paraffin embedded. Then, 8-μm sections were cut, dewaxed, and stained with hematoxylin-eosin solution for morphological analysis. Immunohistochemistry was performed on dewaxed sections by using the automated staining processor system Discovery (Ventana Medical Systems) according to the manufacturer's instructions. The primary antibodies used were to cyclin D1 (polyclonal), PCNA (clone PC10; Santa Cruz Biotechnology, Inc.), monoclonal anti-$p27^{Kip1}$ (BD Transduction Laboratories), and anti-activated caspase 3 (Cell Signaling Technology). Sections were developed by using diaminobenzidine and counterstained with hematoxylin.

Quantitative RT-PCR. RNA was isolated from whole adult testis by using TRIzol (Invitrogen) according to the manufacturer's instructions. Complementary DNA was synthesized from 1 μg of total RNA with the Superscript III First-Strand Synthesis kit (Invitrogen) with random hexamer primers. Quantitative PCR for Aurora C and the housekeeping gene HPRT were performed with a LightCycler instrument and DNA Master SYBR Green I kit (Roche). Primers were as follows: Aurora C forward, 5′-CCAGCACCTCAACCAGGAA-3′; Aurora C reverse, 5′-CCAGCAGTTCATAGCAGAGC; HPRT forward, 5′-CCTG CTGGATTACATTAAAGCACTG; and HPRT reverse, 5′-GTCAAGGGCAT ATCCAACAACAAAC. Serial dilutions of the amplicon were used in the reaction to generate a standard curve, and the specific nature of the PCR was verified through melting curve analysis and by running the product on a 1.5% agarose-TAE gel. Control reactions which had not been incubated with reverse transcriptase (RT) were also included to demonstrate the PCR was specific for the Aurora C transcript. Primer annealing temperatures were 60°C for Aurora C and 58°C for HPRT; all other cycling conditions were as suggested by the LightCycler instrument manufacturers (Roche). The relative amount of Aurora C transcript was then corrected against the relative amount of control HPRT transcript.

RESULTS

Targeted disruption of the PLZP gene. To study the in vivo function of the *PLZP* gene we disrupted it in murine 129/Sv ES cells by homologous recombination. Mouse PLZP is a protein of 465 amino acids that shares high homology with its human counterpart, especially in the BTB/POZ and zinc finger domains (Fig. 1A). We isolated the mouse *PLZP* gene locus from a 129/Sv mouse genomic phage library and characterized it by restriction mapping, direct sequencing, and in silico analysis. We identified another gene located just 1.1 kb downstream of the *PLZP* gene. This neighboring gene is a homologue of the *MLL1* (for mixed lineage leukemia 1) gene involved in acute myeloid and lymphoid leukemia and has recently been described and named *MLL2* (19). Between the two genes we found a CpG island-rich region, which might act as a site for transcriptional regulation (36) (Fig. 1B). Given the organization of this locus, we reasoned that removal of the *PLZP* gene DNA coding sequences and the presence of a neomycin selectable marker cassette would likely also affect transcription of *MLL2* (33). We therefore decided to construct two different targeting vectors to inactivate the *PLZP* gene.

We constructed one targeting vector bearing a neomycin resistance gene to replace the entire coding region of the *PLZP* gene plus a 3′-flanking sequence of 750 bp within the CpG island-rich region (neo vector) (Fig. 2A). We also generated a second targeting vector in which we inserted the *Escherichia coli* β-galactosidase (*lacZ*) reporter gene in frame distal to the *PLZP* gene translation start site, together with a neomycin cassette and Cre recombinase gene contained within two LoxP sites (*lacZ* vector). Expression of Cre recombinase in this construct was under the control of the mouse testis-specific angiotensin-converting enzyme isoform (t-Ace) gene promoter (8) to allow excision of the neomycin cassette plus Cre during passage through the germ line (Fig. 2B). Two (neo vector) and four (lacZ vector) independent, homologous recombinant ES cell clones were used to generate chimeric mice, which transmitted the disrupted allele to the germ line. Identification of the correct recombination events in ES cells and the null mutation of PLZP in the mice were made with two different probes (Fig. 2C and D). Removal of the Neo/t-ACE-Cre cassette was verified by PCR on genomic DNA comparing wild-type, neo vector, and lacZ vector targeted ES cell clones and F_1 heterozygote mice (Fig. 2E). A PCR-based strategy was also developed to genotype the *PLZP* lacZ mutant mice (Fig. 2F). To confirm the null mutation, expression of PLZP mRNA was evaluated by using Northern blot analysis on testis of mice from both the neo (not shown) and lacZ lines (Fig. 2G).

PLZP knockout mice from the neo and lacZ lines were born healthy and developed normally. No gross pathological abnormalities were found. From the offspring of 12 *PLZP* heterozygote breeding pairs (6 neo and 6 lacZ), we observed a distribution of the three genotypes ($PLZP^{+/+}$, $PLZP^{+/-}$, and $PLZP^{-/-}$) according to expected Mendelian ratios (data not shown). To avoid possible interference of the neomycin cassette with the expression of the *MLL2* gene, we nevertheless focused our attention on the lacZ line, henceforth referred to as $PLZP^{wt/wt}$, $PLZP^{wt/lacZ}$, and $PLZP^{lacZ/lacZ}$ mice.

In vivo *lacZ* expression in $PLZP^{wt/lacZ}$ mice. To investigate the in vivo pattern of PLZP expression, we performed β-galactosidase staining on different tissues from $PLZP^{wt/lacZ}$ mice, together with $PLZP^{wt/wt}$ controls. The lacZ-staining pattern in $PLZP^{wt/lacZ}$ mice showed the highest level of expression in the testis, both in tissue sections and in cytological samples by FACS analysis of cell suspensions (Fig. 3A and B and data not shown). The pattern of lacZ staining in testis sections demonstrated that PLZP expression is restricted to the intermediate layers of the germinal epithelium.

As PLZP is expressed in spleens, lymph nodes, and lymphoid cell lines (unpublished data), we checked lacZ expression in lymphocytes from $PLZP^{wt/lacZ}$ mice. We did not find a significant number of lacZ-positive cells under steady-state conditions in samples prepared from spleens, lymph nodes,

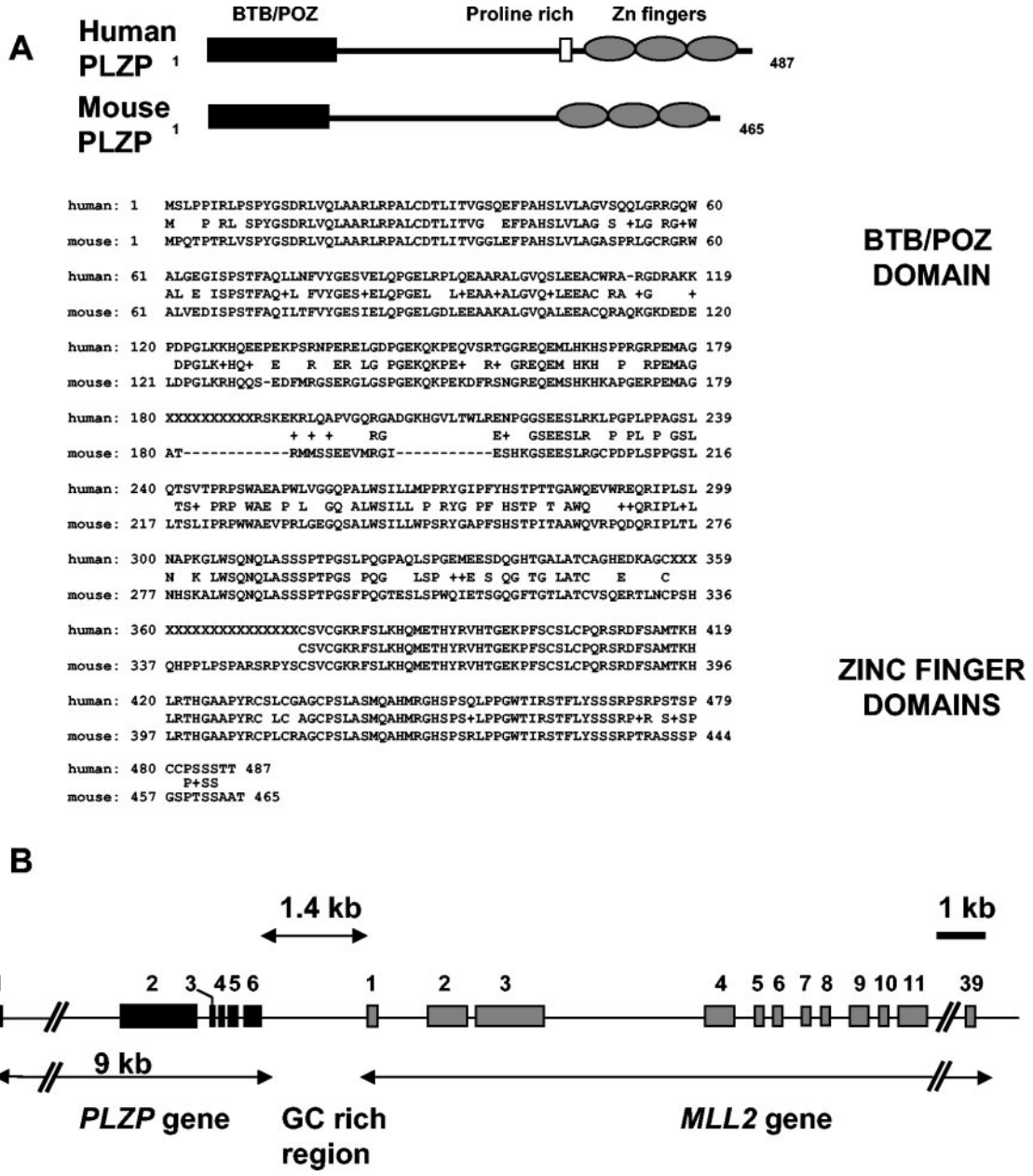

FIG. 1. Characterization of mouse *PLZP* genomic region. (A) Comparison of the structures and sequences of mouse and human PLZP proteins. (B) Schematic representation of the mouse *PLZP* gene locus. The mouse *PLZP* gene is made of six exons spanning ca. 9 kb. Immediately downstream of PLZP (ca. 1.2 kb), the mouse ortholog of the *MLL2* gene is depicted.

and thymuses (data not shown). However, in both $CD4^+$ and $CD8^+$ T lymphocytes, PLZP transcription was upregulated as early as 12 h after TCR engagement with anti-CD3 antibodies and peaked by 24 h, as evaluated by FDG staining and FACS analysis (Fig. 3C, middle panels). The addition of anti-CD28 antibody to the cultures enhanced the FDG signal, especially at 24 h, suggesting that the CD28-dependent costimulatory pathway might be involved in the control of *PLZP* gene transcription (Fig. 3C, bottom panels). Moreover, other mitogenic stimuli, such as concanavalin A and calcium ionophore (calcimycin) coupled to PMA gave the same upregulation of *PLZP* expression in T cells (data not shown and Fig. 3D, left panel). The addition of cyclosporine, a potent inhibitor of T-lymphocyte activation, attenuated but did not abolish lacZ expression, suggesting that *PLZP* transcription might partially be under control of cyclosporine-sensitive pathways (Fig. 3D, right panel). In this regard, we analyzed the 5′-flanking region of the *PLZP* gene and identified multiple potential target sites of transcription factors involved in early transcriptional events after activation of T lymphocytes. These transcription factors include NF-κB and interestingly, NFAT, which is a target of cyclosporine (data not shown). Stimulation of B lymphocytes with various mitogens did not show upregulation of lacZ fluorescence (data not shown).

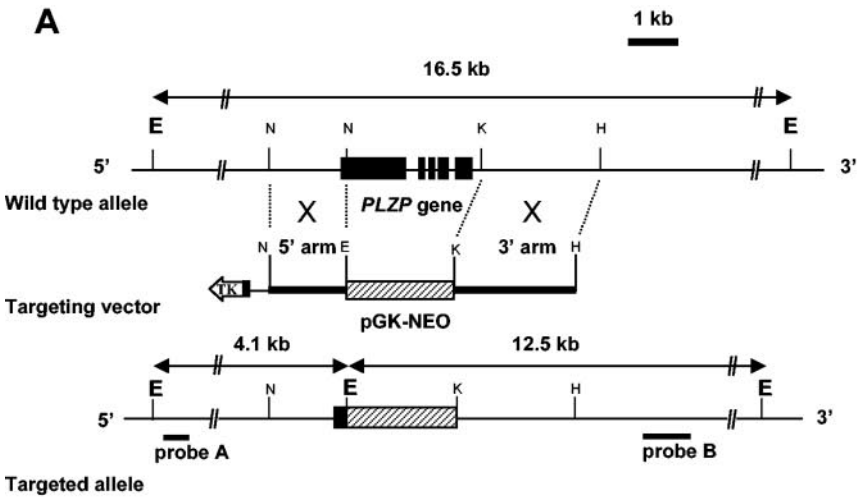
A
1 kb
16.5 kb
E
N
N
K
H
E
5'
3'
Wild type allele
PLZP gene
N 5' arm E
K
3' arm H
TK
Targeting vector
pGK-NEO
4.1 kb
12.5 kb
probe A
probe B
Targeted allele

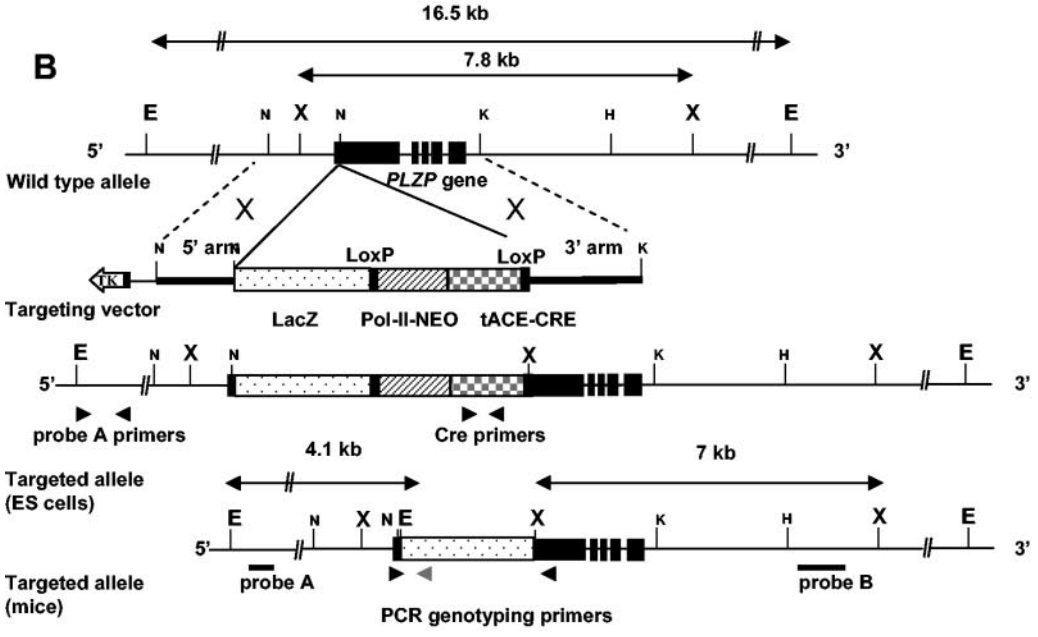
B
16.5 kb
7.8 kb
E
N
X
N
K
H
X
E
5'
3'
Wild type allele
PLZP gene
5' arm
LoxP
LoxP
3' arm
TK
Targeting vector
LacZ
Pol-II-NEO
tACE-CRE
probe A primers
Cre primers
4.1 kb
7 kb
Targeted allele
(ES cells)
probe A
probe B
Targeted allele
(mice)
PCR genotyping primers

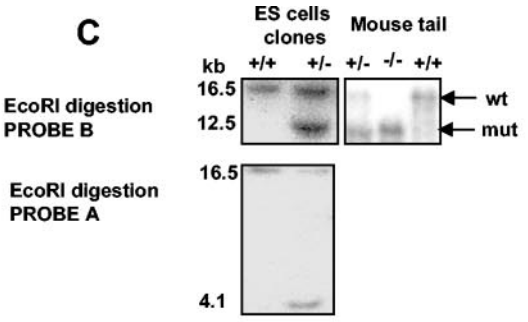
C
ES cells
clones
Mouse tail
kb
+/+
+/-
+/-
-/-
+/+
EcoRI digestion
PROBE B
16.5
12.5
wt
mut
EcoRI digestion
PROBE A
16.5
4.1

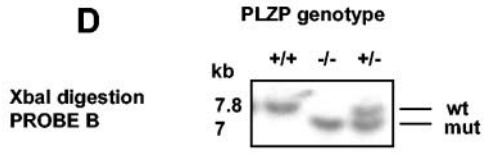
D
PLZP genotype
+/+
-/-
+/-
kb
XbaI digestion
PROBE B
7.8
7
wt
mut

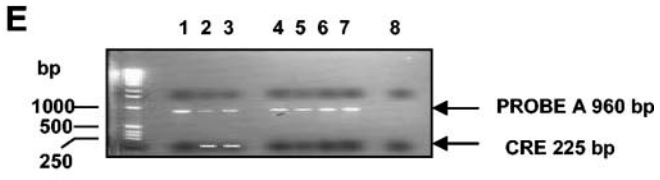
E
1 2 3
4 5 6 7
8
bp
1000
500
250
PROBE A 960 bp
CRE 225 bp

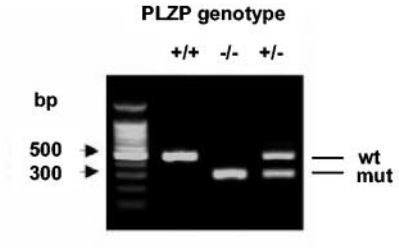
PLZP genotype
+/+
-/-
+/-
F
bp
500
300
wt
mut

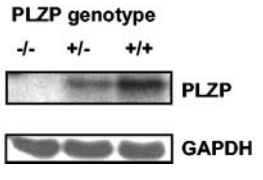
PLZP genotype
-/-
+/-
+/+
G
PLZP
GAPDH

FIG. 2. Mouse *PLZP* gene targeting strategy. (A and B) Targeting vectors and scheme of homologous recombination in the knockout that replaces PLZP sequences with a neo cassette (A) or the neo-cre-lacZ cassette insertional knockout (B). (C) Southern blot analysis on EcoRI-digested genomic DNA with 5′ and 3′ external probes (probe A and probe B in the scheme) demonstrating homologous recombination in the ES cells (the same strategy is used for ES cells transfected with the neo cassette or the neo-cre-lacZ cassette vectors) and germ line transmission to the PLZP-neo mice. (D) Southern blot demonstrating germ line transmission of the PLZP-lacZ mice. (E) Multiplex PCR on genomic DNA extracted from wild-type ES cells (lane 1), two recombined ES cell clones with the neo-cre-lacZ vector (lanes 2 and 3), four F_1 mice generated from these ES cell clones bearing the floxed PLZP allele (lanes 4 to 7), and a water control (lane 8). The 960-bp band corresponds to the 5′ external probe A amplified as an internal control, whereas the 225-bp band corresponds to a fragment of the Cre gene in the neo-cre-lacZ vector, which has been excised in the F_1 mice. (F) Genotyping of lacZ vector mice by multiplex PCR of extracted tail DNA. The 500-bp product represents the wild-type locus, while the 300-bp represents lacZ insertion into the *PLZP* locus. (G) Northern blot for the PLZP gene on total RNA extracted from testes of −/−, +/−, and +/+ *lacZ* vector mice, showing absence of transcripts in −/− mice. Restriction enzyme sites abbreviations: E, EcoRI; K, KpnI; H, HindIII; N, NdeI; X, XbaI.

We next assessed the pattern of *PLZP* expression in mouse hematopoietic precursors. We therefore FACS-sorted lineage$^-$ (Lin$^-$) Sca1$^+$ and Lin$^+$ Sca1$^+$ BM cells from *PLZP*$^{wt/lacZ}$ mice and stained them for lacZ expression. In the Lin$^+$ Sca1$^+$ sorted cell population, which contains mostly committed progenitors, we could detect only rare lacZ$^+$ stained cells (not shown). However, in the Sca1$^+$ Lin$^-$ sorted stem cell population, we observed an enrichment of lacZ-stained cells (Fig. 3E). Taken together, these findings demonstrate that murine PLZP is most highly expressed in the germinal epithelium of the testis, in activated T lymphocytes and in the hematopoietic stem cell (HSC)-enriched Sca1$^+$ Lin$^-$ fraction of BM cells.

Normal testis development and structure in PLZP-null mice. The human homologue of mouse *PLZP* was originally cloned from testis, where it was found to be highly expressed (27), hence it was originally given the name testis zinc-finger protein (TZFP). Indeed, through monitoring expression of the β-galactosidase reporter gene in our mice, which is controlled by the *PLZP* promoter, we can demonstrate a high level of expression in the seminiferous tubules of the testis as shown above (Fig. 3A). *PLZP*$^{lacZ/lacZ}$ mice were fertile, arguing against a significant defect in spermatogenesis and/or spermiogenesis. To perform a more detailed analysis, sections of testis from *PLZP*$^{lacZ/lacZ}$ and wild-type littermate controls were immunostained for a variety of markers of proliferation, apoptosis and for the distinct cell populations within the tubules (Fig. 4A). Morphology of the *PLZP*$^{lacZ/lacZ}$ testis appeared grossly normal, plus sperm were being generated normally within the tubules suggestive of an intact differentiation pathway of the spermatogonia into spermatids. The spermatogonia within the tubules were intact, as judged by a specific marker for this population, PCNA (40). In addition, both spermatogonia proliferation and apoptosis appeared unaffected in the *PLZP*$^{lacZ/lacZ}$ testis, as determined by cyclin D1 expression and activated Caspase-3 staining, respectively (6, 21). The numbers of supporting Sertoli cells in *PLZP*$^{lacZ/lacZ}$ testis could also be confirmed to be similar to those found in the wild type by immunostaining for p27^{kip}, a marker for this cell type (5). A specific function for PLZP in testis has previously been suggested; a testis-specific member of the Aurora Ser/Thr kinase family, Aurora C (AIE1), is reported to be transcriptionally repressed by PLZP (38). The Aurora family kinases are thought to be critical regulators of the cell cycle (7, 9), and Aurora C is known to be expressed in meiotically active spermatocytes within the testis (24), overlapping with the expression pattern of PLZP (Fig. 3A). We therefore sought to determine whether loss of PLZP led to a derepression of Aurora C expression. However, analysis of Aurora C transcript levels in *PLZP*$^{lacZ/lacZ}$ testis by quantitative RT-PCR showed no significant upregulation of this gene (Fig. 4B). Thus, it is either possible that Aurora C is not a bona fide target for PLZP in vivo or that additional transcriptional repressors can substitute for PLZP in regulation of Aurora C expression.

PLZP deficiency does not result in gross hematopoietic abnormalities or in defects of the DNA damage response of hematopoietic progenitors. The pattern of PLZP expression in hematopoietic organs as well as in early hematopoiesis suggested a potential function in these compartments. We there-

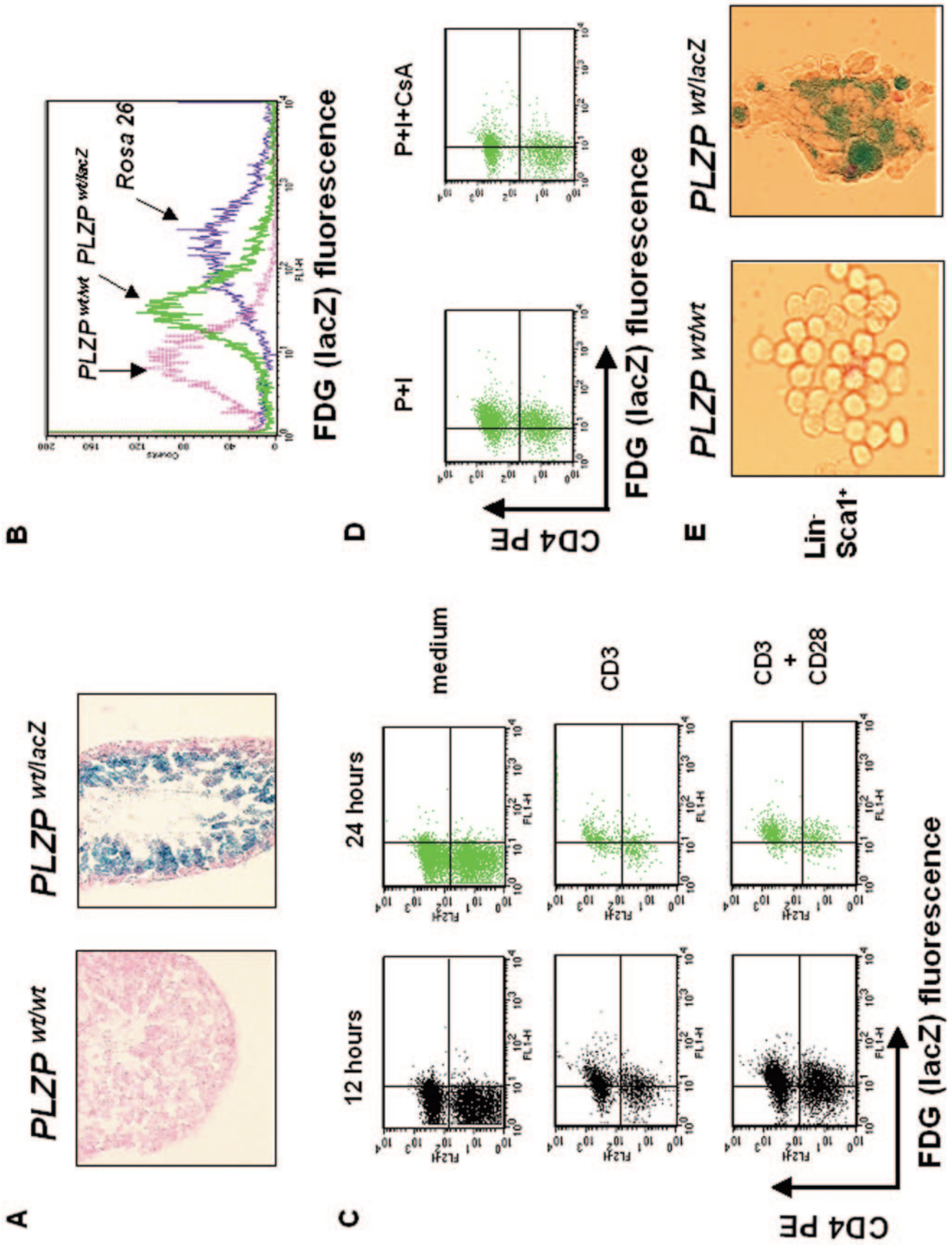
A
PLZP wt/wt
PLZP wt/lacZ
B
PLZP wt/wt
PLZP wt/lacZ
Rosa 26
FDG (lacZ) fluorescence
C
12 hours
24 hours
medium
CD3
CD3 + CD28
CD4 PE
FDG (lacZ) fluorescence
D
P+I
P+I+CsA
CD4 PE
FDG (lacZ) fluorescence
E
PLZP wt/wt
PLZP wt/lacZ
Lin-
Sca1+

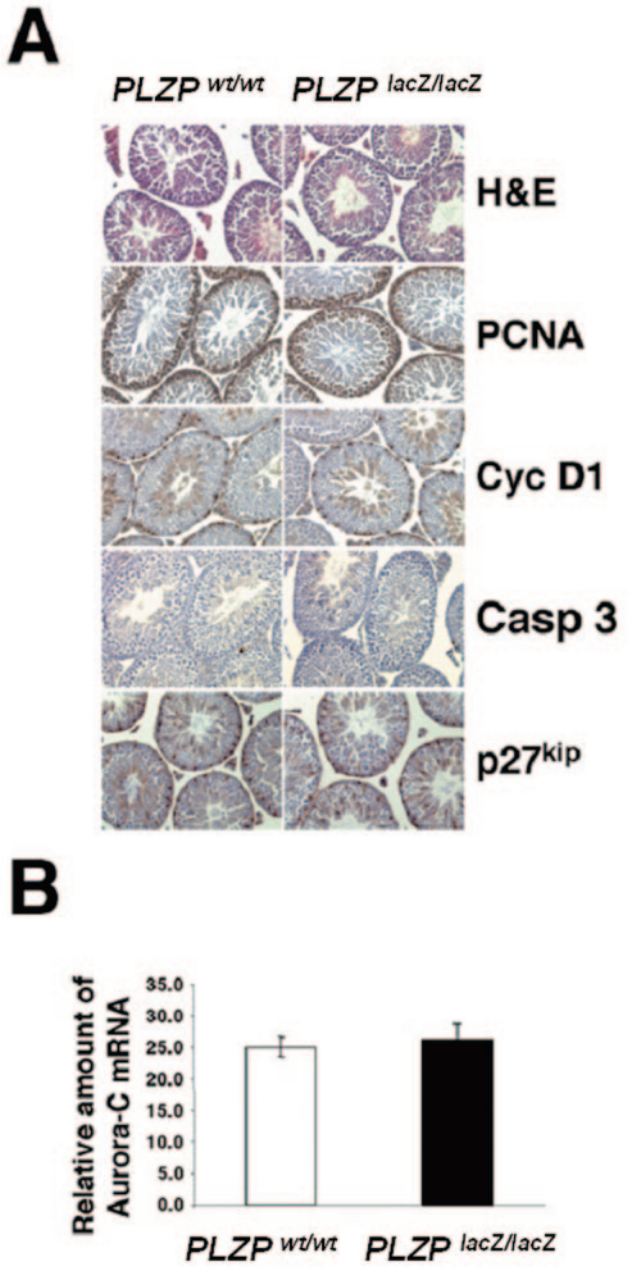

FIG. 4. Analysis of testis from adult $PLZP^{lacZ/lacZ}$ and $PLZP^{wt/wt}$ mice. (A) Representative images of testis stained with hematoxylin and eosin (H&E) to show morphology and stained with a variety of antibodies by immunohistochemistry (from upper to lower panels: PCNA, cyclin D1, activated caspase 3, and $p27^{kip}$). Scale bar, 5 μm. (B) Quantitative RT-PCR analysis of Aurora C expression in testis extracts from $PLZP^{wt/wt}$ and $PLZP^{lacZ/lacZ}$ adult mice. Testis extracts from three $PLZP^{lacZ/lacZ}$ mice, together with three littermate $PLZP^{wt/wt}$ controls, were analyzed, and the mean values of relative expression are shown ± the standard errors.

FIG. 3. In vivo expression pattern of PLZP-lacZ. (A) LacZ staining of testis tissue sections showing *lacZ*-positive (blue) cells in the intermediate layers of the germinal epithelium. (B) FACS analysis of FDG staining (see Materials and Methods) of testis germinal cells isolated from wild-type, $PLZP^{wt/lacZ}$, and control Rosa 26 mice. (C) Flow cytometry analysis of $PLZP^{wt/lacZ}$ total ($CD3^+$ sorted) T lymphocytes after TCR stimulation with anti-CD3 and anti-CD3 plus anti-CD28 antibodies at 12 and 24 h. Cells were stained for CD4-PE (FL-2) and for FDG (FL-1) to detect β-galactosidase activity. (D) $PLZP^{wt/lacZ}$ total ($CD3^+$ sorted) T lymphocytes stimulated with PMA plus ionomycin (P+I) or PMA plus ionomycin and cyclosporine were stained with FDG and analyzed by flow cytometry. (E) LacZ staining of BM sorted cells from wild-type and $PLZP^{wt/lacZ}$ mice. Lin^- and $Sca1^+$ cells were sorted by FACS, stained for β-galactosidase activity, and then analyzed.

fore undertook a thorough analysis of the hematopoietic system in PLZP mutant mice.

The BM, peripheral blood, and lymphoid organs of $PLZP^{wt/wt}$, $PLZP^{wt/lacZ}$, and $PLZP^{lacZ/lacZ}$ mice were analyzed by FACS immunophenotyping for lymphoid, erythroid and myeloid cell

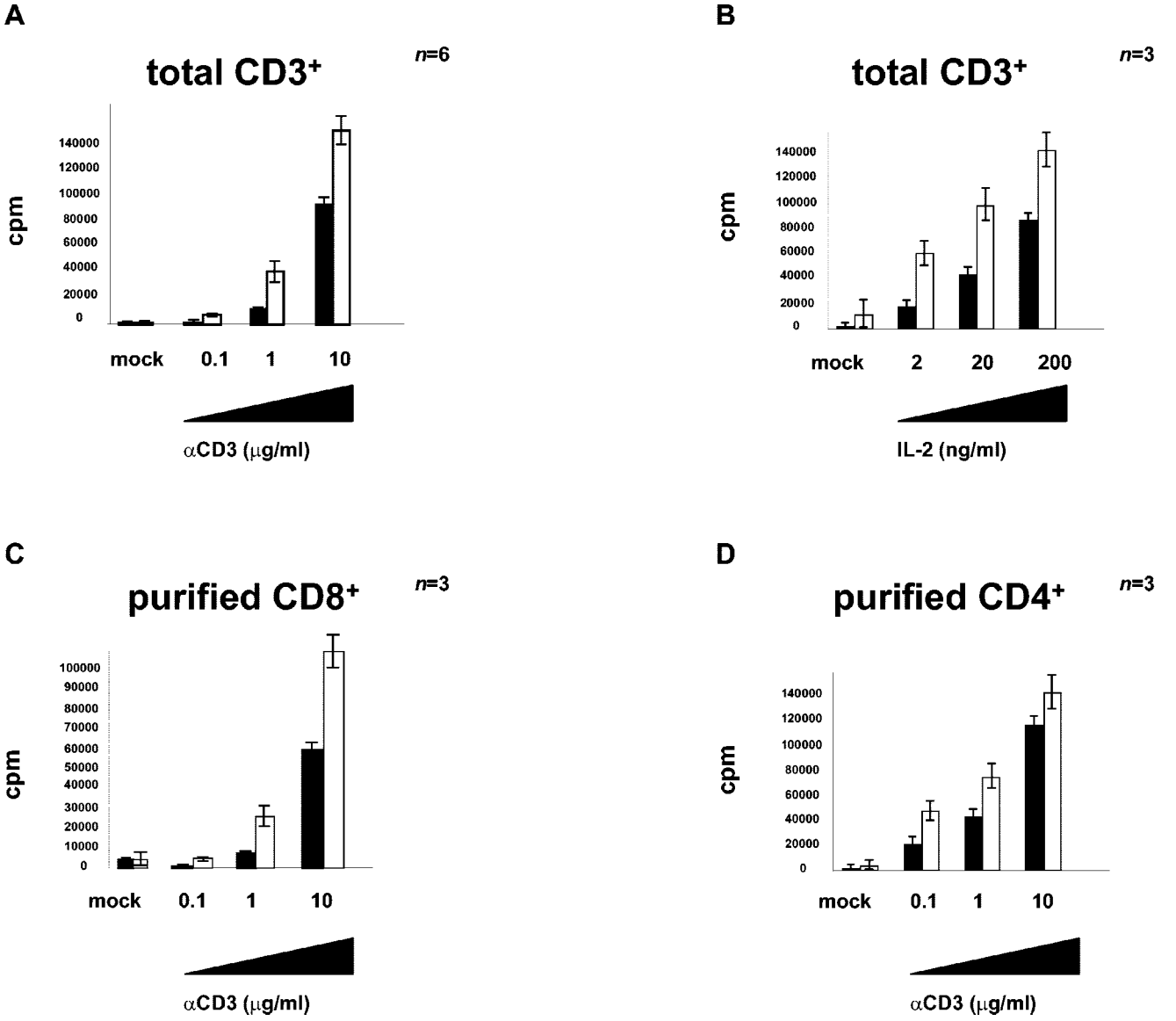

FIG. 5. T-lymphocyte dysfunction in *PLZP*$^{lacZ/lacZ}$ mice. (A and B) Increased proliferation of PLZP-deficient total T lymphocytes (CD3$^+$ sorted) upon TCR (anti-CD3ε) (A) and IL-2 (B) stimulation. (C and D) Increased proliferation of sorted CD8$^+$ (C) and CD4$^+$ (D) *PLZP*$^{lacZ/lacZ}$ T lymphocytes upon TCR (anti-CD3ε) engagement. The data are mean values of the counts per minute ± the standard errors (n = six or three mice for each genotype). Black bars, wild-type lymphocytes; white bars, *PLZP*$^{lacZ/lacZ}$ lymphocytes.

surface markers, as well as by pathological examination. Peripheral blood automated and differential cell counts were comparable in both young (4- to 8-week-old) and older (12- to 15-month-old) mice of the three genotypes (data not shown). The distribution of B cells, T cells, and myeloid cell subsets in the peripheral blood, BM, and primary and secondary lymphoid organs were unaltered in *PLZP*$^{lacZ/lacZ}$ animals compared to the respective sex-matched control littermates. We therefore concluded that PLZP inactivation in the mouse does not result in gross alteration in development of the hematopoietic system.

Since PLZP has been shown to physically interact with FANC-C, we wanted to test whether the response of *PLZP*$^{lacZ/lacZ}$ hematopoietic progenitors to DNA damage, which is significantly impaired in FANC-C knockout mice and in patients with mutations in the FANC-C gene, could be affected. To test this hypothesis, we irradiated or treated with mitomycin C BM cells from *PLZP*$^{lacZ/lacZ}$ and *PLZP*$^{wt/wt}$ mice and subsequently evaluated the colony-forming potential of hematopoietic progenitors by colony-forming cell assay. However, we could not demonstrate any significant difference in the sensitivities of *PLZP*$^{lacZ/lacZ}$ and *PLZP*$^{wt/wt}$ cells to these stimuli (data not shown). We therefore concluded that the hematopoietic progenitor cell response to gamma irradiation and mitomycin C-induced DNA damage is not altered in *PLZP*$^{lacZ/lacZ}$ mice.

Increased proliferative response of PLZP knockout T lymphocytes. Given that the expression of PLZP is increased after

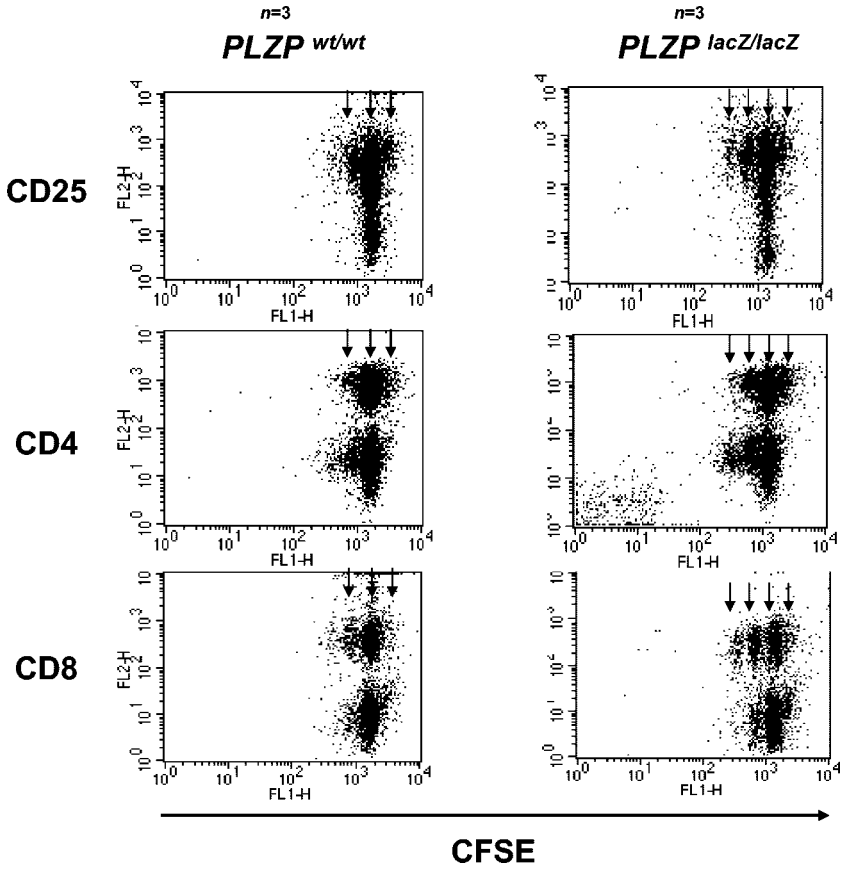

FIG. 6. Increased cell divisions in T lymphocytes from *PLZP*$^{lacZ/lacZ}$. Total (CD3$^+$ sorted) T lymphocytes from *PLZP*$^{wt/wt}$ and *PLZP*$^{lacZ/lacZ}$ mice were labeled with CFSE and stimulated for 72 h with plate-bound anti-CD3ε (2 μg/ml) plus IL-2 (100 ng/ml). Cells were subsequently stained with anti-CD4, -CD8, and -CD25-PE MAbs and analyzed for the number of cell divisions by flow cytometry. One of three independent experiments is represented (n = three mice for each genotype).

activation of both CD4$^+$ and CD8$^+$ T lymphocytes (see above), we hypothesized that PLZP could play a role in the regulation of T-cell proliferation. We therefore assessed the proliferation of *PLZP*$^{lacZ/lacZ}$ and *PLZP*$^{wt/wt}$ control T lymphocytes upon TCR engagement. The proliferative response of *PLZP*$^{lacZ/lacZ}$ CD3$^+$ T lymphocytes to increasing concentrations of αCD3 antibody was enhanced compared to controls (Fig. 5A). Moreover, at a lower (suboptimal) concentration of αCD3 antibody (0.05 μg/ml), *PLZP*$^{lacZ/lacZ}$ T lymphocytes displayed a stronger proliferative response to increasing IL-2 stimulation compared to the wild type (Fig. 5B). This increased proliferation was observed at early time points (24 h) and was also maintained at later time points (72-96 h) (data not shown). When analyzed individually, both the CD4$^+$- and the CD8$^+$-T-lymphocyte subtypes demonstrated an increased response to TCR triggering, and this was particularly evident with the CD8$^+$ cells (Fig. 5C and D). To further characterize the increased proliferative response displayed by *PLZP*$^{lacZ/lacZ}$ T lymphocytes, we evaluated the number of cell divisions of stimulated *PLZP*$^{lacZ/lacZ}$ and *PLZP*$^{wt/wt}$ T lymphocytes by CFSE labeling and FACS analysis. We found that a higher number of *PLZP*$^{lacZ/lacZ}$ T cells, both CD4$^+$ and CD8$^+$, displayed, on average, one more cell division after 72 to 96 h from stimulation (Fig. 6). These data demonstrate that PLZP is involved in the control of proliferation of both CD4$^+$ and CD8$^+$ T lymphocytes and strongly suggests that PLZP plays a role during the early response of T cells to TCR stimulation.

Deregulated cytokine production in T cells from PLZP-null mice. We next investigated the mechanisms by which PLZP inactivation would lead to increased T-cell proliferation. Since mouse PLZP has been shown to repress the transcription of growth-inhibitory cytokines such as IFN-γ in transient-transfection reporter assays. In similar assays, PLZP was also shown to repress IL-4 transcription (30). We therefore determined whether cytokine transcription was affected by the absence of PLZP. We stimulated purified CD4$^+$ and CD8$^+$ T lymphocytes from *PLZP*$^{lacZ/lacZ}$ and *PLZP*$^{wt/wt}$ littermate controls under neutral, T-helper 1 and T-helper 2 skewing conditions and assessed the levels of cytokines by intracellular staining and FACS analysis or by RNase protection assays. In this series of experiments, we observed that CD8$^+$ *PLZP*$^{lacZ/lacZ}$ T lymphocytes, stimulated under neutral conditions, produced more IFN-γ (Fig. 7A), whereas CD4$^+$ T lymphocytes, stimulated under T-helper 2 skewing conditions, expressed higher levels of IL-4, IL-5, and IL-13 transcripts compared to controls (Fig. 7B).

Increased metabolic activity and altered homeostasis of hemopoietic stem cells/progenitor pool in *PLZP*-null mice. We

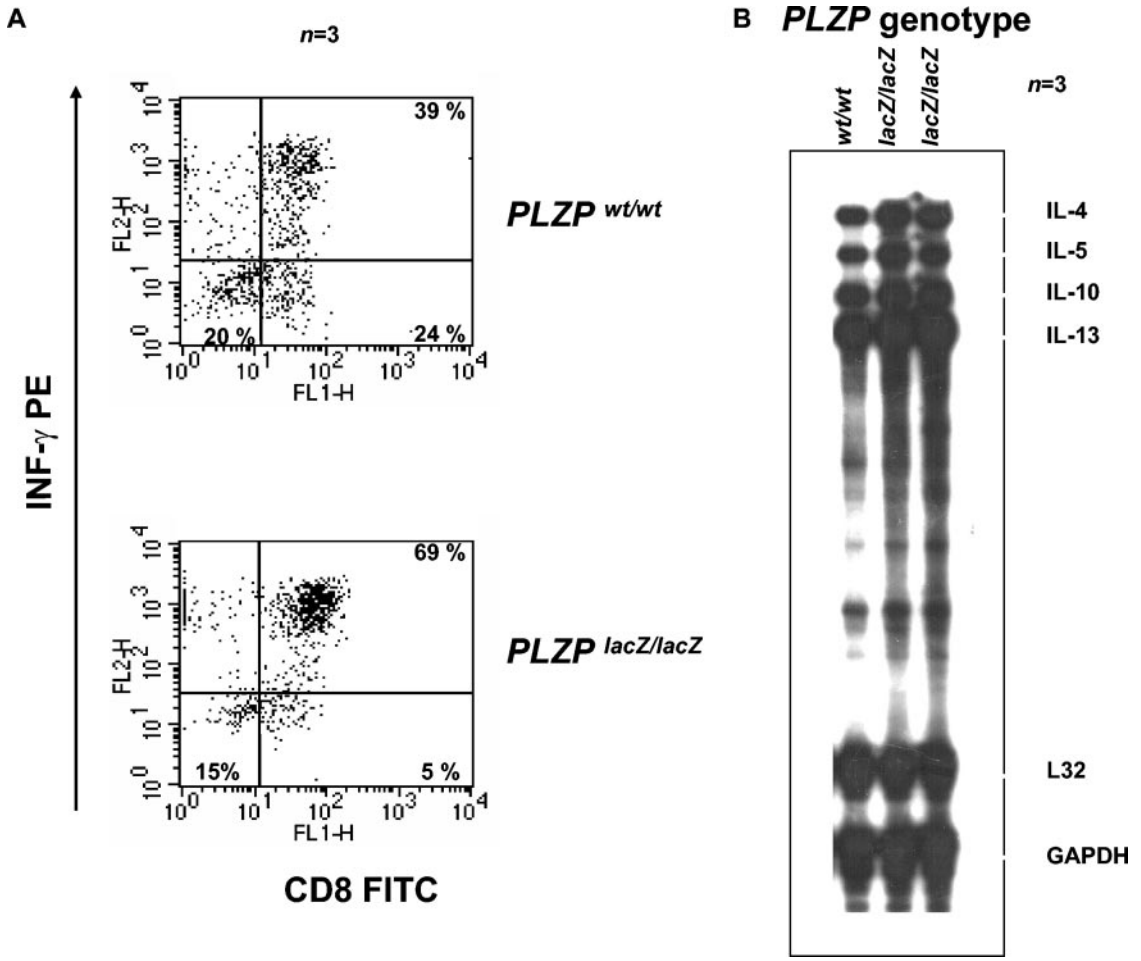

FIG. 7. Enhanced cytokine production by $PLZP^{lacZ/lacZ}$ T lymphocytes. (A) Intracellular staining of $PLZP^{wt/wt}$ (top panel) and $PLZP^{lacZ/lacZ}$ (bottom panel) $CD8^+$ T lymphocytes for IFN-γ after activation with CD3 plus CD28 and IL-2. (B) RNase protection assays for different Th2-type cytokine mRNAs from $CD4^+$ T lymphocytes grown in Th-2 skewing conditions. One of three independent experiments is represented (n = three mice for each genotype).

next quantified the functional population of hematopoietic progenitors by using CFC assays in $PLZP^{wt/wt}$ and $PLZP^{lacZ/lacZ}$ mice under steady-state conditions. However, we did not observe any significant difference in BFU-E, CFU-GM, and CFU-GEMM colony numbers between $PLZP^{lacZ/lacZ}$ and $PLZP^{wt/wt}$ BM cells grown in the presence of a complete cytokine cocktail (data not shown).

PLZP is expressed in HSC/early progenitors, and a potential role for PLZP, along with PLZF, in regulating proliferation in this compartment has been proposed (14). We therefore assessed this possible role of PLZP by analyzing the proliferative status of HSCs and the ratio between quiescent and metabolically active cell pools in $PLZP^{lacZ/lacZ}$ and $PLZP^{wt/wt}$ mice. We performed cell cycle fractionation experiments with four-parameter flow cytometry analysis on total BM cells assessing the cell cycle status (i.e., quiescent versus cycling cells) of the progenitor pool by staining with Pyronin Y, together with Hoechst 33342, to measure RNA and DNA content, respectively (13). In fact, it has been previously demonstrated that elevated intracellular RNA levels associate with cell cycle entry, whereas cell cycle phase is given by DNA content. We found that the HSC/early progenitor pool (as defined as $Sca1^+$ Lin^- Hoechst 33342^{low}) present in the $PLZP^{lacZ/lacZ}$ BM contains a significantly higher percentage of pyronin Y $(PY)^{hi}$-stained cells, which are exiting from the quiescent pool and entering cell division, compared to $PLZP^{wt/wt}$ (Fig. 8A). The ratio between quiescent progenitors in G_0 and cells that have entered cell cycle in G_1 was lower for the $PLZP^{lacZ/lacZ}$ progenitors than for the $PLZP^{wt/wt}$ controls (Fig. 8B). PLZP is therefore regulating the proliferative rate and the balance between metabolically active and inactive cells of the HSC or progenitor pool at the steady state.

DISCUSSION

PLZP is a novel BTB/POZ protein that displays a high degree of homology with the PLZF protein. Human PLZP physically interacts with FANC-C and PLZF and has therefore been proposed to have possible involvement in the pathogenesis of Fanconi's anemia and APL. In the present study we describe an analysis of mice in which the PLZP gene has been targeted by homologous recombination. This analysis allowed

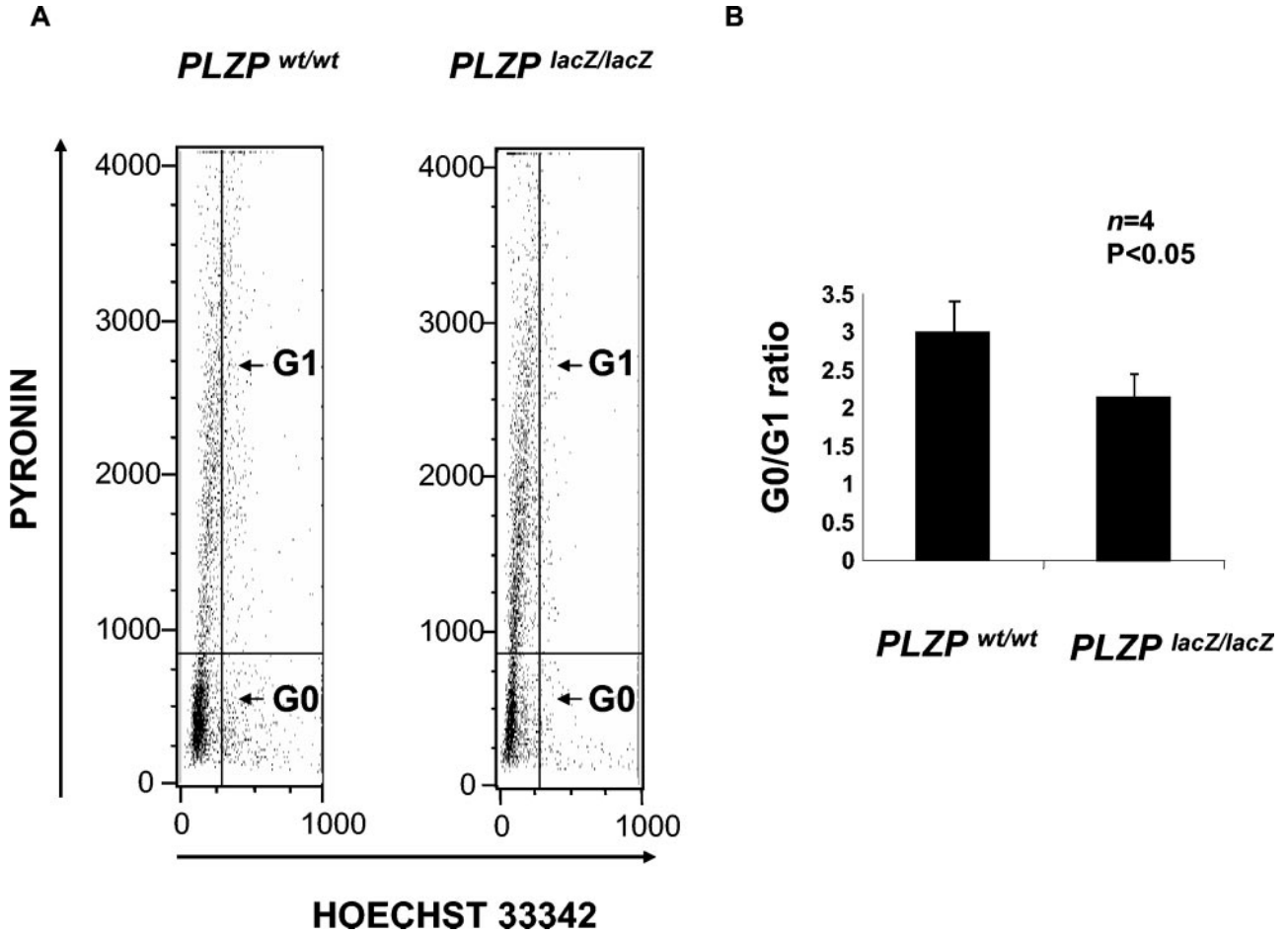

FIG. 8. HSC pools in G_0 and G_1 phases of the cell cycle in PLZP-deficient mice. (A) Analysis of total BM cells stained for Sca1 and lineage antibodies, pyronin (RNA), and Hoechst (DNA) reveals an increased proportion of progenitors ($Sca1^+$ Lin^-) in G_1 of the cell cycle (PY+) in $PLZP^{lacZ/lacZ}$ mice compared to controls. (B) Average of the ratio of percentage of cells in G_0 versus G_1 is plotted. The data represent the mean value ± the standard errors ($n = 4$; $P < 0.05$).

us to demonstrate that PLZF and PLZP exert distinct, albeit overlapping, functions.

The similarity between PLZF and PLZP is already apparent at the genomic level. As for PLZF (42), the genomic region containing the *PLZP* gene is highly conserved in mammals as demonstrated by the striking homology between the human and mouse DNA sequences. The *PLZP* gene is located very close to the trithorax homolog *MLL2*/*MLL4*, and this region (on chromosome 19q13.1) appears to be phylogenetically very close to the genomic region, which contains the *PLZF* and the *MLL1* genes (on chromosome 11q23) (36, 42). Intriguingly, both regions are involved in rearrangements in cancer (http://cgap.nci.nih.gov).

We were able to assess the pattern of *PLZP* expression by analyzing the expression of a *lacZ* reporter gene knocked into the mouse *PLZP* locus. We demonstrate that this gene is expressed in activated $CD4^+$ and $CD8^+$ T lymphocytes, the germinal epithelium of the testis and the $Sca1^+$ Lin^- subfraction of HSCs. Our results extend beyond previous descriptions of the expression pattern of mouse PLZP (30). In the testis, we find that unlike PLZF that is expressed in spermatogonia (14), PLZP is mainly expressed in the intermediate maturation layers in histological sections, in which the prevailing cell population is represented by primary and secondary spermatocytes. PLZP is expressed in the $Sca1^+$ Lin^- fraction of HSCs, which also contain early myeloid progenitors. PLZP and PLZF display an overlapping pattern of expression in the mouse HSC compartment. They are both highly expressed in human $CD34^+$ progenitors and levels are progressively reduced along the myeloerythroid differentiation pathway (15).

Our in vivo functional analysis reveals striking differences between the two transcription factors but also important similarities. We found, for instance, that unlike PLZF, PLZP is dispensable for normal mouse development and spermatogenesis. This is explained in part by the fact that PLZP is not expressed in the developing limb and axial skeletal structures (F. Piazza and P. P. Pandolfi, unpublished observations), whereas the lack of phenotype in the PLZP-null testis may suggest a functional redundancy and a more prominent role for PLZF. However, we found that PLZP regulates the proliferative activity of T lymphocytes and is involved in control of the balance between quiescent and cycling pools of HSCs, a function that is shared with PLZF (J. A. Costoya et al. unpublished observations).

Analysis of testes from $PLZP^{lacZ/lacZ}$ and $PLZP^{wt/wt}$ mice did not reveal abnormalities of testis function or development in $PLZP^{lacZ/lacZ}$ mice. A thorough analysis of several testis-specific markers of maturation and function also showed no alterations in $PLZP^{lacZ/lacZ}$ mice. Moreover, the levels of a suggested PLZP testis-specific target gene, Aurora kinase, *AIE1*, were not affected by the absence of PLZP. The reasons for high PLZP expression in the testis may be related to other processes not obvious to our analysis. Alternatively, it is possible that other factors, such as PLZF, may compensate for PLZP deficiency in the testis, but this is perhaps unlikely since, as mentioned earlier, PLZF and PLZP are expressed at different stages of spermatogenesis (14).

We have also established a role for PLZP in the control of cellular proliferation in the hematopoietic compartment. $PLZP^{lacZ/lacZ}$ T lymphocytes, both CD4 and CD8, displayed increased proliferation upon stimulation. In addition, we demonstrated that the production of cytokines was deregulated in the absence of PLZP. $CD8^+$ $PLZP^{lacZ/lacZ}$ T-lymphocytes produce more IFN-γ upon TCR stimulation and $CD4^+$ T lymphocytes stimulated under T-helper 2-type conditions produce more Th2-type cytokines. However, this mechanism must be compensated for in vivo, since $PLZP^{lacZ/lacZ}$ mice do not develop spontaneous immune-mediated or inflammatory manifestations during their life span. In keeping with our findings, PLZP-induced inhibition of T-cell activation and proliferation was recently described in a T-cell-specific PLZP transgenic mouse (31). Intriguingly, another BTB/POZ protein, BCL-6, has been shown to act as a negative regulator of effector T-lymphocyte function. BCL-6-deficient mice spontaneously develop a systemic inflammatory disease characterized by an increased T-helper 2 response (41). Moreover, BCL-6 is involved in the regulation of GATA-3 expression and T-helper 2 development (25). It is tempting to speculate on a possible functional interaction between PLZP and BCL-6 in the regulation of this developmental pathway.

Analysis of cell cycle and metabolic activity in HSCs from $PLZP^{lacZ/lacZ}$ BM showed increased numbers of cells in G_1 phase versus the G_0 phase under steady-state conditions, as evaluated by Hoechst and Pyronin Y staining of the $Sca1^+$ Lin^- population of BM cells. However, $PLZP^{lacZ/lacZ}$ HSC and progenitor cells did not show alterations in their ability to produce colonies of the differing hemopoietic lineages in vitro. These results therefore suggest that loss of PLZP affects mainly the self-renewal or differentiation kinetics of the HSC/progenitors and is likely more related with the long-term repopulating capability of the HSCs (12, 13).

The control of proliferation, self-renewal, and differentiation of HSCs is a fundamental process that is actively studied because of its clinical and therapeutic implications, since it is well known that the HSCs have a limited proliferative potential (20, 32). Recent studies have outlined the fundamental role of cell cycle inhibitors such as p21 and p27 in the regulation of the HSC compartment homeostasis (12, 13). The absence of these regulators, despite little or absent impact on hematopoiesis, has a profound effect on the homeostasis of HSC/early progenitor compartment. The long-term repopulating potential of HSCs is profoundly impaired in $p21^{-/-}$ mice, whereas the short-term repopulating capability is markedly impaired in $p27^{-/-}$ mice. Our data indicate that the HSC/progenitor cells in $PLZP^{lacZ/lacZ}$ mice show increased cell cycling activity but without a clinically evident phenotype throughout the life span of the mouse. Important follow-up experiments (such as competitive repopulation or serial BM transplantation assays) should be performed to further investigate the role of PLZP in regulating HSC/progenitor cell activity. However, the sensitive flow cytometric analysis of BM cells we describe here allow us to conclude that there is a significant perturbation of HSC/progenitor cell homeostasis in $PLZP^{lacZ/lacZ}$ mice at the steady state. It also remains to be determined to which extent PLZF compensates for PLZP loss in this critical function.

ACKNOWLEDGMENTS

We are grateful to M. Capecchi for the pACN vector; M. Barna, A. Di Cristofano, C. Gurrieri, D. Ruggero, and P. Salomoni for helpful discussions; the Transgenic and Genomic, Molecular Cytology, Flow Cytometry, and Molecular Pathology Core facilities for technical assistance; and the members of the Molecular and Developmental Biology Laboratory.

This study was supported in part by a grant from the National Institute of Health (RO1-CA-71692) to P.P.P.

REFERENCES

1. **Albagli, O., P. Dhordain, C. Deweindt, G. Lecocq, and D. Leprince.** 1995. The BTB/POZ domain: a new protein-protein interaction motif common to DNA- and actin-binding proteins. Cell Growth Differ. **6:**1193–1198.
2. **Bardwell, V. J., and R. Treisman.** 1994. The POZ domain: a conserved protein-protein interaction motif. Genes Dev. **8:**1664–1677.
3. **Barna, M., N. Hawe, L. Niswander, and P. P. Pandolfi.** 2000. Plzf regulates limb and axial skeletal patterning. Nat. Genet. **25:**166–172.
4. **Barna, M., T. Merghoub, J. A. Costoya, D. Ruggero, M. Branford, A. Bergia, B. Samori, and P. P. Pandolfi.** 2002. Plzf mediates transcriptional repression of HoxD gene expression through chromatin remodeling. Dev. Cell **3:**499–510.
5. **Beumer, T. L., H. Kiyokawa, H. L. Roepers-Gajadien, L. A. van den Bos, T. M. Lock, I. S. Gademan, D. H. Rutgers, A. Koff, and D. G. de Rooij.** 1999. Regulatory role of $p27^{kip1}$ in the mouse and human testis. Endocrinology **140:**1834–1840.
6. **Beumer, T. L., H. L. Roepers-Gajadien, I. S. Gademan, H. B. Kal, and D. G. de Rooij.** 2000. Involvement of the D-type cyclins in germ cell proliferation and differentiation in the mouse. Biol. Reprod. **63:**1893–1898.
7. **Bischoff, J. R., and G. D. Plowman.** 1999. The Aurora/Ipl1p kinase family: regulators of chromosome segregation and cytokinesis. Trends Cell Biol. **9:**454–459.
8. **Bunting, M., K. E. Bernstein, J. M. Greer, M. R. Capecchi, and K. R. Thomas.** 1999. Targeting genes for self-excision in the germ line. Genes Dev. **13:**1524–1528.
9. **Carmena, M., and W. C. Earnshaw.** 2003. The cellular geography of aurora kinases. Nat. Rev. Mol. Cell. Biol. **4:**842–854.
10. **Chen, S. J., A. Zelent, J. H. Tong, H. Q. Yu, Z. Y. Wang, J. Derre, R. Berger, S. Waxman, and Z. Chen.** 1993. Rearrangements of the retinoic acid receptor alpha and promyelocytic leukemia zinc finger genes resulting from t(11; 17)(q23;q21) in a patient with acute promyelocytic leukemia. J. Clin. Investig. **91:**2260–2267.
11. **Chen, Z., F. Guidez, P. Rousselot, A. Agadir, S. J. Chen, Z. Y. Wang, L. Degos, A. Zelent, S. Waxman, and C. Chomienne.** 1994. PLZF-RAR alpha fusion proteins generated from the variant t(11;17)(q23;q21) translocation in acute promyelocytic leukemia inhibit ligand-dependent transactivation of wild-type retinoic acid receptors. Proc. Natl. Acad. Sci. USA **91:**1178–1182.
12. **Cheng, T., N. Rodrigues, D. Dombkowski, S. Stier, and D. T. Scadden.** 2000. Stem cell repopulation efficiency but not pool size is governed by $p27^{kip1}$. Nat. Med. **6:**1235–1240.
13. **Cheng, T., N. Rodrigues, H. Shen, Y. Yang, D. Dombkowski, M. Sykes, and D. T. Scadden.** 2000. Hematopoietic stem cell quiescence maintained by $p21^{cip1/waf1}$. Science **287:**1804–1808.
14. **Costoya, J. A., R. M. Hobbs, M. Barna, G. Cattoretti, K. Manova, M. Sukhwani, K. E. Orwig, D. J. Wolgemuth, and P. P. Pandolfi.** 2004. Essential role of Plzf in maintenance of spermatogonial stem cells. Nat. Genet. **36:** 653–659.
15. **Dai, M. S., N. Chevallier, S. Stone, M. C. Heinrich, M. McConnell, T. Reuter, H. E. Broxmeyer, J. D. Licht, L. Lu, and M. E. Hoatlin.** 2002. The effects of the Fanconi anemia zinc finger (FAZF) on cell cycle, apoptosis, and proliferation are differentiation stage-specific. J. Biol. Chem. **277:**26327–26334.
16. **David, G., L. Alland, S. H. Hong, C. W. Wong, R. A. DePinho, and A. Dejean.**

1998. Histone deacetylase associated with mSin3A mediates repression by the acute promyelocytic leukemia-associated PLZF protein. Oncogene **16:** 2549–2556.
17. **Dhordain, P., R. J. Lin, S. Quief, D. Lantoine, J. P. Kerckaert, R. M. Evans, and O. Albagli.** 1998. The LAZ3(BCL-6) oncoprotein recruits a SMRT/mSIN3A/histone deacetylase containing complex to mediate transcriptional repression. Nucleic Acids Res. **26:**4645–4651.
18. **Dong, S., J. Zhu, A. Reid, P. Strutt, F. Guidez, H. J. Zhong, Z. Y. Wang, J. Licht, S. Waxman, C. Chomienne, et al.** 1996. Amino-terminal protein-protein interaction motif (POZ-domain) is responsible for activities of the promyelocytic leukemia zinc finger-retinoic acid receptor-alpha fusion protein. Proc. Natl. Acad. Sci. USA **93**:3624–3629.
19. **FitzGerald KT, D. M.** 1999. MLL2: a new mammalian member of the trx/MLL family of genes. Genomics **59**:187–192.
20. **Geiger, H., and G. Van Zant.** 2002. The aging of lympho-hematopoietic stem cells. Nat. Immunol. **3:**329–333.
21. **Gown, A. M., and M. C. Willingham.** 2002. Improved detection of apoptotic cells in archival paraffin sections: immunohistochemistry using antibodies to cleaved caspase 3. J. Histochem. Cytochem. **50:**449–454.
22. **He, L. Z., M. Bhaumik, C. Tribioli, E. M. Rego, S. Ivins, A. Zelent, and P. P. Pandolfi.** 2000. Two critical hits for promyelocytic leukemia. Mol. Cell **6:**1131–1141.
23. **Hoatlin, M. E., Y. Zhi, H. Ball, K. Silvey, A. Melnick, S. Stone, S. Arai, N. Hawe, G. Owen, A. Zelent, and J. D. Licht.** 1999. A novel BTB/POZ transcriptional repressor protein interacts with the Fanconi anemia group C protein and PLZF. Blood **94:**3737–3747.
24. **Hu, H. M., C. K. Chuang, M. J. Lee, T. C. Tseng, and T. K. Tang.** 2000. Genomic organization, expression, and chromosome localization of a third aurora-related kinase gene, Aie1. DNA Cell Biol. **19:**679–688.
25. **Kusam, S., L. M. Toney, H. Sato, and A. L. Dent.** 2003. Inhibition of Th2 differentiation and GATA-3 expression by BCL-6. J. Immunol. **170:**2435–2441.
26. **Licht, J. D., R. Shaknovich, M. A. English, A. Melnick, J. Y. Li, J. C. Reddy, S. Dong, S. J. Chen, A. Zelent, and S. Waxman.** 1996. Reduced and altered DNA-binding and transcriptional properties of the PLZF-retinoic acid receptor-alpha chimera generated in t(11;17)-associated acute promyelocytic leukemia. Oncogene **12:**323–336.
27. **Lin, W., C. H. Lai, C. J. Tang, C. J. Huang, and T. K. Tang.** 1999. Identification and gene structure of a novel human PLZF-related transcription factor gene, TZFP. Biochem. Biophys. Res. Commun. **264:**789–795.
28. **Lo Coco, F., B. H. Ye, F. Lista, P. Corradini, K. Offit, D. M. Knowles, R. S. Chaganti, and R. Dalla-Favera.** 1994. Rearrangements of the BCL6 gene in diffuse large cell non-Hodgkin's lymphoma. Blood **83:**1757–1759.
29. **MacGregor, G. R., B. P. Zambrowicz, and P. Soriano.** 1995. Tissue nonspecific alkaline phosphatase is expressed in both embryonic and extraembryonic lineages during mouse embryogenesis but is not required for migration of primordial germ cells. Development **121:**1487–1496.
30. **Miaw, S. C., A. Choi, E. Yu, H. Kishikawa, and I. C. Ho.** 2000. ROG, repressor of GATA, regulates the expression of cytokine genes. Immunity **12:**323–333.
31. **Miaw, S. C., B. Y. Kang, I. A. White, and I. C. Ho.** 2004. A repressor of GATA-mediated negative feedback mechanism of T-cell activation. J. Immunol. **172:**170–177.
32. **Morrison, S. J., D. E. Wright, S. H. Cheshier, and I. L. Weissman.** 1997. Hematopoietic stem cells: challenges to expectations. Curr. Opin. Immunol. **9:**216–221.
33. **Olson, E. N., H. H. Arnold, P. W. Rigby, and B. J. Wold.** 1996. Know your neighbors: three phenotypes in null mutants of the myogenic bHLH gene MRF4. Cell **85:**1–4.
34. **Omori, M., Y. M., M. Inami, M. Ukai-Tadenuma, Y. M. Kimura, Nigo, H. Hosokawa, A. Hasegawa, and T. Nakayama.** 2003. CD8 T cell-specific downregulation of histone hyperacetylation and gene activation of the IL-4 gene locus by ROG, repressor of GATA. Immunity **19:**281–294.
35. **Piazza, F., T. Merghoub, and P. Pandolfi.** 1999. Characterization of PLZP, a novel PLZF-related factor. Blood **94:**1145.
36. **Piazza, F., T. Merghoub, and P. Pandolfi.** 2001. High Conservation in mammals of a genomic region containing two homologous of acute myeloid leukemia-associated genes PLZF and MLL. Blood **98:**416.
37. **Sitterlin, D., P. Tiollais, and C. Transy.** 1997. The RAR alpha-PLZF chimera associated with acute promyelocytic leukemia has retained a sequence-specific DNA-binding domain. Oncogene **14:**1067–1074.
38. **Tang, C. J., C. K. Chuang, H. M. Hu, and T. K. Tang.** 2001. The zinc finger domain of Tzfp binds to the tbs motif located at the upstream flanking region of the Aie1 (aurora-C) kinase gene. J. Biol. Chem. **276:**19631–19639.
39. **Tsuzuki, S., and T. Enver.** 2002. Interactions of GATA-2 with the promyelocytic leukemia zinc finger (PLZF) protein, its homologue FAZF, and the t(11;17)-generated PLZF-retinoic acid receptor alpha oncoprotein. Blood **99:**3404–3410.
40. **Wrobel, K. H., D. Bickel, and R. Kujat.** 1996. Immunohistochemical study of seminiferous epithelium in adult bovine testis using monoclonal antibodies against Ki-67 protein and proliferating cell nuclear antigen (PCNA). Cell Tissue Res. **283:**191–201.
41. **Ye, B. H., G. Cattoretti, Q. Shen, J. Zhang, N. Hawe, R. de Waard, C. Leung, M. Nouri-Shirazi, A. Orazi, R. S. Chaganti, P. Rothman, A. M. Stall, P. P. Pandolfi, and R. Dalla-Favera.** 1997. The BCL-6 proto-oncogene controls germinal-centre formation and Th2-type inflammation. Nat. Genet. **16:**161–170.
42. **Zhang, T., H. Xiong, L. X. Kan, C. K. Zhang, X. F. Jiao, G. Fu, Q. H. Zhang, L. Lu, J. H. Tong, B. W. Gu, M. Yu, J. X. Liu, J. Licht, S. Waxman, A. Zelent, E. Chen, and S. J. Chen.** 1999. Genomic sequence, structural organization, molecular evolution, and aberrant rearrangement of promyelocytic leukemia zinc finger gene. Proc. Natl. Acad. Sci. USA **96:**11422–11427.